

# Designing Fast Quantum Gates with Tunable Couplers: A Reinforcement Learning Approach

Bijita Sarma<sup>1,\*</sup> and Michael J. Hartmann<sup>1,2</sup>

<sup>1</sup>Department of Physics, Friedrich-Alexander-Universität Erlangen-Nürnberg, 91058 Erlangen, Germany

<sup>2</sup>Max Planck Institute for the Science of Light, 91058 Erlangen, Germany

Fast quantum gates are crucial not only for the contemporary era of noisy intermediate-scale quantum devices but also for the prospective development of practical fault-tolerant quantum computing systems. Leakage errors, which arise from data qubits jumping beyond the confines of the computational subspace, are the main challenges in realizing non-adiabatically driven, fast gates. In this letter, we propose and illustrate the usefulness of reinforcement learning (RL) to generate fast two-qubit gates in practical multi-level superconducting qubits. In particular, we show that the RL controller offers great effectiveness in finding piecewise constant gate pulse sequences autonomously that act on two transmon data qubits coupled by a tunable coupler to generate a controlled-Z (CZ) gate with 11 ns gate time and an error rate of  $\sim 4 \times 10^{-3}$ , making it about five times faster than state-of-the-art implementations. Such gate pulse sequences exploit the leakage space judiciously by controlling the leakage dynamics into and out of the computational subspace at appropriate times during the gate application, making it extremely fast.

As we are inching closer to building practical quantum computers, the development of fast quantum gates has become increasingly important [1]. This is instrumental in the current noisy intermediate-scale quantum (NISQ) era, to allow quantum algorithms to be executed reliably despite the inherent noise and fragility of qubits, as well as to achieve fault-tolerant quantum computing with efficient error-correcting gate implementations in larger systems [2–8]. Fault-tolerance means that, provided the error rates of the physical qubits are below a threshold, quantum computing devices, along with quantum error correction (QEC) and logical gate operations, would be able to be used for practical quantum computation [9–12]. One of the crucial requirements for efficient QEC is the realization of fast and efficient quantum gates [13].

As a hardware platform for quantum computing, superconducting circuits have shown remarkable developments and are considered promising for constructing large-scale quantum devices. However, despite recent advancements in such quantum hardware components, designing high fidelity and at the same time fast gates, remains a major challenge. Since superconducting qubits are in fact multi-level systems, the most significant challenge in achieving fast two-qubit gates is avoiding leakage errors that results from qubits leaking out of the computational basis [14–17]. These leakage errors have proven to be particularly hard to correct, and strategies to avoid them limit the amplitude of control pulses, which makes that gate duration longer despite optimization of gate pulse sequences.

Another major problem for the precise operation of large-scale superconducting platforms is crosstalk originating from residual ZZ-interactions, which causes unwanted perturbations to two-qubit gate operations. One way to reduce crosstalk is to improve the hardware design, such as by utilizing qubits with opposite anharmonicities to create a quantum interference-induced crosstalk-cancellation effect [18–20]. The more experimentally favorable way would be to park the qubits at a highly dispersive regime with large detunings. Nevertheless, in such setups, when transitioning from a far-off detuning to an operating zone of frequencies with reduced detuning, the gates become slower. This work proposes a solu-

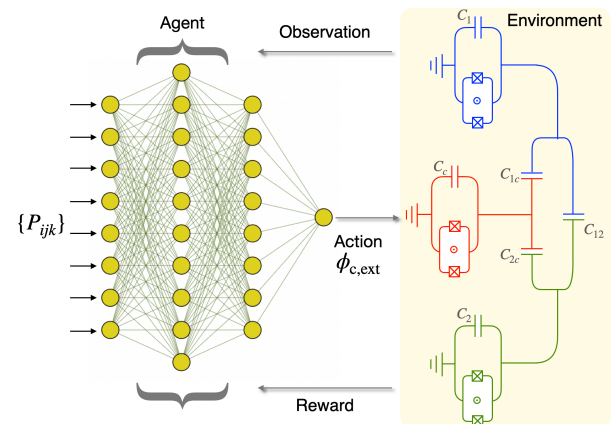


Figure 1. Schematic diagram showing the RL-controlled gate implementation in a three-qubit tunable coupler circuit. The circuit (right), which constitutes the RL-environment, is made of three transmon superconducting qubits, each modelled by a multi-level anharmonic oscillator, with capacitive nearest-neighbour and next-nearest neighbor couplings. The RL agent is fed with observations  $\{P_{ijk}\}$ , here the computational and leakage-space qubit populations. Based on these observations, the agent exerts actions to control the coupler frequency,  $\omega_c(t)$  and receives an according reward or penalty in terms of the gate infidelity  $\mathcal{I} = 1 - \mathcal{F}$ , where  $\mathcal{F}$  is the gate fidelity at the end of the sequence.

tion for realizing fast two-qubit gate that starts from a regime where residual couplings are low, and even though the ramps are sharp, the optimization algorithm leads to a fast gate.

When dealing with global optimization problems of complex, non-convex, and non-linear systems, machine learning (ML) in combination with deep learning has recently proven to be extremely successful and is considered highly versatile for a wide range of tasks [21]. Reinforcement learning (RL) is a type of ML that is particularly well suited for learning to control sequential decision-making problems [22]. Unlike supervised (unsupervised) learning which relies on labeled (unlabeled) datasets, RL learns through interactions with the sys-

tem to be controlled (called the RL environment). The RL model, called the RL-agent receives rewards or punishments as feedback that guide its learning process and allow it to adapt and improve over time. This has made RL invaluable in areas such as robotics, autonomous systems, and games, where agents need to learn optimal strategies through trial and error, outperforming supervised learning in complex, dynamic environments with superhuman capabilities. [23, 24]. Following such developments in technology and various domains in engineering, it has recently been utilized to find control protocols in the domains of quantum physics for some interesting quantum systems [25, 26]. It was first demonstrated for the optimization of quantum state preparations [27] and QEC [28], and more recently we have seen its applications in other areas, in particular, in quantum state engineering [29], quantum state transfer [30], quantum feedback control [31–33], etc. RL controls have also been used in real laboratory experiments recently with quantum systems, demonstrating their potential for challenging decisions and their adaptability to control such systems in real time [34, 35].

In this Letter, we propose and analyze a method to design an ultrafast two-qubit controlled-Z (CZ) gate using RL-based optimization in a tunable coupler superconducting circuit setup, see Fig. 1. Besides being an entangling gate that can be used to generate a universal gate set, the CZ gate is a core operation in QEC with surface codes, where stabilizers can be measured via a sequence of four CZ gates [10, 13]. For engineering high performance, large-scale quantum processors, tunable superconducting circuits have gained prominence, particularly due to their recently recognized capability for on-demand on-off switching of couplings between qubit pairs via frequency modulation through external flux [13, 19, 36, 37]. This flexibility allows for precise control over the interactions within the system, making it a valuable resource for implementing high fidelity gates. We find that the RL-agent could autonomously discover high performance control pulses, while considering all leakage sub-spaces. Such coherent-error-avoiding flux pulses judiciously control the qubit leakage dynamics into and out of the computational subspace at appropriate times during the course of the gate, making it extremely fast. With this approach, we show that an ultrafast CZ gate can be realized with a gate-time of 11 ns with an error rate  $\sim 4 \times 10^{-3}$ .

The RL-based optimization protocol we consider is depicted in Fig. 1, where the problem of two-qubit gate design with tunable coupler superconducting framework is embedded into the workflow of RL. The RL-agent (shown on the left) is essentially an artificial neural network model that is responsible for deciding the control sequences (called the actions,  $\vec{a}$ ) by optimizing the weights,  $\vec{\theta}$  of the model. These optimizations are directed through the scalar signal of rewards,  $\mathcal{R}$  received by the RL-agent from the RL-environment given it observes some partial information of the system after the application of the control at every step of iteration. These are called the observations,  $\vec{s}$  of the RL, and the set of rules it learns by optimizing the parameters  $\vec{\theta}$  is called the policy,

$\pi(\vec{a}|\vec{s})$  of the RL-agent, where  $\pi(\vec{a}|\vec{s})$  represents a conditional probability distribution of  $\vec{a}$  given  $\vec{s}$ . In this case, the RL-environment comprises the tunable coupler circuit, shown on the right of Fig. 1, comprising two data qubits and a coupler qubit, all of which are modeled as transmon qubits. Explicitly, the observation of the RL-agent consists of the computational as well as leakage-space qubit populations, i.e.,  $\vec{s} = \{P_{ijk}\}$ , where  $i, j, k = (0, 1, 2)$  are the indices corresponding to the energy levels of the three qubits, with  $j$  being the levels of the tunable coupler qubit. The actions of the RL-agent are choices of the tunable coupler frequency,  $\omega_c$ , which are realized by the external flux,  $\phi_{c,\text{ext}}$  applied to the coupler, therefore  $\vec{a} = \{\omega_c\} \leftarrow \phi_{c,\text{ext}}$ . The reward,  $\mathcal{R}$  is considered as a function of the process infidelity of the CZ gate defined by  $\mathcal{R} = -\log_{10}(1 - \mathcal{F})$ , where  $\mathcal{F}$  is the gate fidelity at the end of the sequence.

The learning process can be divided into iterations (called episodes) of total duration  $\tau$  which is divided into sequences of duration  $t = \tau/n$ , where  $n$  is the number of control steps in the sequence. If we consider a control problem with  $N_a$  control parameters over  $n$  control steps, the complexity of the problem scales exponentially with  $n$  as  $N_a \prod_{i=1}^{N_a} N_i^n$ , where  $N_i$  is the number of divisions for the  $i$ -th control parameter, considering a discrete control problem. For the problem under study  $N_a = 1$ , for which the complexity of the problem scales as  $N_{\omega_c}^n$ , where  $N_{\omega_c}$  is the number of divisions of the control parameter  $\omega_c$ . Instead of discrete controls, we consider continuous approximations to stepwise constant shapes of  $\omega_c$ . This choice of control pulses is motivated by the fact that they are typical pulses generated by arbitrary waveform generators in current experimental setups.

Despite the fact that we have a single control parameter for the RL-agent to learn, this problem turned out to be a formidable task for the RL to learn and we have found that a sophisticated RL algorithm developed in the last few years needs to be employed. Effectively, we used the recently proposed Soft-Actor-Critic (SAC) algorithm for optimization of the RL policy [38]. SAC algorithm is an actor-critic RL algorithm based on the concept of entropy regularization, where the policy  $\pi$  is trained to maximize a trade-off between expected return and entropy that determines the balance between exploration and exploitation, receiving a bonus reward at each time step proportional to the entropy of the policy. This makes the RL-policy to spawn  $m$  actions as randomly as possible due to the inherent stochasticity of the policy, encouraging the agent towards more exploration, prevention of premature convergence to sub-optimal solutions, and accelerated learning. The optimal policy  $\pi^*$  is defined as the policy that maximizes the expected return while also maximizing entropy, given by

$$\pi^* = \underset{\pi}{\operatorname{argmax}} \mathbb{E}_{\tau \sim \pi} \sum_{t=0}^{\infty} \gamma^t [\mathcal{R}(s_t, a_t, s_{t+1}) + \alpha \mathcal{H}(\pi(\cdot|s_t))], \quad (1)$$

where  $\mathbb{E}_{\tau \sim \pi}$  denotes the expectation value over trajectories  $\tau$  generated by following the policy  $\pi$ .  $\gamma^t$  is the discount factor

raised to the power of  $t$ , where  $\gamma$  is a parameter between 0 and 1, representing how much the agent values future rewards relative to immediate rewards.  $\mathcal{R}(s_t, a_t, s_{t+1})$  term represents the immediate reward obtained when taking action  $a_t$  in state  $s_t$  and transitioning to state  $s_{t+1}$ . The  $\alpha \mathcal{H}(\pi(\cdot|s_t))$  term involves the entropy  $\mathcal{H}$  of the policy  $\pi$  at state  $s_t$ , weighted by a hyper-parameter  $\alpha$ , that regulates stochasticity of the policy, and encourages randomness in the actions taken by the RL-agent.

The tunable coupler circuit depicted in Fig. 1 is described by the Hamiltonian (considering  $\hbar = 1$  hereinafter),

$$H = \sum_{i=1,c,2} \left( \omega_i b_i^\dagger b_i + \frac{\alpha_i}{2} b_i^\dagger b_i^\dagger b_i b_i \right) + g_{12} (b_1^\dagger b_2 + b_2^\dagger b_1) + \sum_{i=1,2} g_{ic} (b_i^\dagger b_c + b_c^\dagger b_i), \quad (2)$$

where  $b_i (b_i^\dagger)$  with  $i = 1, c, 2$  describe the bosonic annihilation (creation) operators for the transmon qubits ( $i = 1, 2$ ) and the coupler, where the qubits are considered as weakly anharmonic oscillators possessing multiple energy levels, with anharmonicities given by  $\alpha_i$ . The qubits interact with one another through capacitive coupling, where the next-nearest-neighbour coupling capacitance,  $C_{12}$ , is smaller than the nearest-neighbour coupling capacitances,  $\{C_{1c}, C_{2c}\}$ , which in turn are small compared to the transmon qubit capacitances  $\{C_1, C_c, C_2\}$ . This leads to the fact that the circuit analysis can be treated perturbatively. The experimentally relevant computational basis of the circuit can be described by the eigenstates  $|ijk\rangle$  at the idling point, where  $\{i, j, k\}$  label the energy levels of the qubit 1, coupler and qubit 2 respectively. Due to the residual coupling at the idle point, these eigenstates are slightly hybridized between the individual circuit components [19]. The computational subspace for the two-qubit gates between the data qubits consists of the states  $|ik\rangle = |00\rangle, |01\rangle, |10\rangle$  and  $|11\rangle$ , where the coupler is considered to be always in the ground state. The circuit is initialized at the eigenstates  $|ijk\rangle$  before application of the gate and is returned back to after the completion of the gate operation, which have maximum overlap with the bare states,  $|i'j'k'\rangle$  of the circuit; whereas all the other instantaneous eigenstates during the gate constitute the leakage subspace.

We aim to design the CZ gate utilizing the transverse qubit-qubit coupling to induce a phase of  $e^{i\pi}$  in the computational state  $|101\rangle$  by using nonadiabatic transitions to the non-computational eigenstate  $|002\rangle$  and back. At the idle point, we consider the qubits to be in the highly dispersive regime where the detuning between the coupler and the qubits is large compared to the couplings, so that both the transverse and longitudinal couplings between the qubits are negligible. However as the frequency of the coupler is brought close to that of the two qubits, with proper choice of circuit parameters, the effective two-qubit transverse coupling can be switched on. We bias the qubits at the frequencies of  $\omega_1/2\pi = 4.2$  GHz,  $\omega_2/2\pi = 5.2$  GHz and  $\omega_c/2\pi = 6.32$  GHz. This results in an almost zero transverse coupling and a negligible ZZ-crosstalk

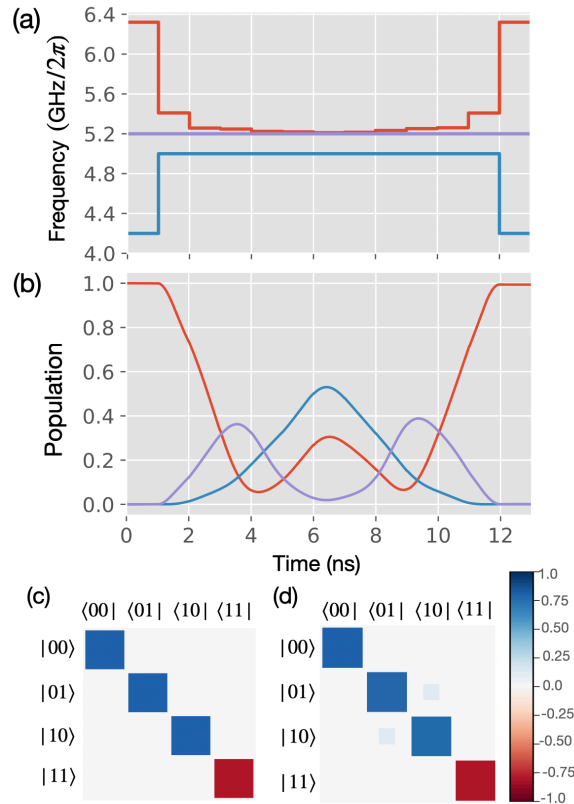


Figure 2. (a) The RL-discovered piecewise constant variations of the coupler qubit transition frequency (red), as well as the frequency dynamics of the data qubit 1 (blue) and the qubit 2 (purple). Before implementation of the gate, the qubits are started at the idle point with negligible crosstalk, and also brought to the same resting configuration after the gate. (b) The corresponding population distribution throughout the gate evolution time in the significantly occupied eigenstates. (c) and (d) show the absolute values of the matrix elements,  $|\langle j, l|U|k, l\rangle|^2$ , in the subspace formed by the two data qubits, for the target gate unitary and the resultant gate unitary.

( $-8.37$  kHz) [see supplemental material for details].

Starting at this dispersive coupling limit, a CZ-gate can be obtained by first tuning the frequency of qubit 1 to  $\omega_1 = \omega_2 + U_{21}$ , so that the levels  $|101\rangle$  and  $|002\rangle$  become resonant, and then tuning the coupler frequency near to the data qubit frequencies. Holding the coupler frequency at this point for the time of one oscillation between these two states, the target unitary  $U_{CZ} = \text{diag}(1, 1, 1, -1)$  can be achieved up to single qubit phases, which can be compensated virtually. However, the gate-time for such a Rabi-oscillation based operation is long as it is given by  $t_{\text{gate}} = \pi/\zeta_{XX}$ , where  $\zeta_{XX}$  is the transverse coupling rate.

To implement a faster gate, we use a RL-based approach as stated above to tune the coupler frequency. Based on observation  $O(t_i)$ , the agent takes action  $A(t_i)$ , which is selecting the frequency of the coupler. Depending on this action, the agent receives either a positive or negative reward, which

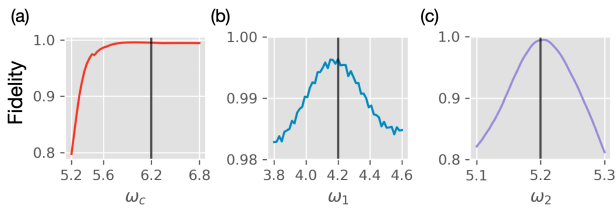


Figure 3. The variation in gate fidelity outcome in response to model fluctuations, expressed in terms of idling (initial) frequencies (in units of  $\text{GHz}/2\pi$ ) for the (a) coupler qubit, (b) qubit 1 and (c) qubit 2 respectively, when employing the identical reinforcement learning-derived pulse as found for the parameters indicated by the black vertical lines.

guides its next move. Therefore, our gate implementation is based solely on reward-based optimization without any initial model for the expected tunable pulse shape. The goal is to quickly drive the qubit transitions to reach the desired unitary while reducing the population of leakage states at the end of the gate.

In Fig. 2 we show the piecewise controls discovered by the RL-agent in panel (a) as well as the population dynamics among the computational and leakage states in panel (b). One can see that the RL-protocol finds very fast control pulses leading to a gate-time of 11 ns where the infidelity can be suppressed to  $\sim 4 \times 10^{-3}$ . For finding this fastest pulse the RL-agent finds optimal conditions where the coupler excited state is also populated during the gate. The leakage population is determined by the detuning of the coupler qubit and is non-zero during the gate, although the population of the leakage states decrease at the end of the gate. Such fast gates are advantageous to overcome the effects of finite qubit lifetime, since the decoherence time for the state of the art transmons is of the order of  $\tilde{\tau} \sim 60 \mu\text{s}$ , leading to error rates characterized by  $\varepsilon_{\tilde{\tau}} = 1 - \exp(-t_{\text{gate}}/\tilde{\tau}) \approx 1 \times 10^{-4}$  [36]. Fig. 2(c) and (d) show the target CZ-unitary distribution as well as the obtained unitary distribution. The most interesting result found by the RL-agent is the intuitive leakage utilization to realize the ultrafast gate. The flux pulse is designed autonomously by the RL-agent in such a way that there is population transfer first from the state  $|101\rangle$  to state  $|111\rangle$  i.e. the coupler, then to the state  $|002\rangle$  with some remaining part in  $|101\rangle$ , then again back to the coupler, and finally to the state  $|101\rangle$ , with the acquired phase of  $\pi$ .

Finally, we discuss the prospects of the proposed method for experimental implementations. To explore its utility in this context, we investigated the applicability of the obtained pulse shapes in devices where the transition frequencies of the qubits do not exactly match the parameters of the assumed model, c.f. Eq. 2. We show the robustness of our method against such parameter fluctuations in Fig. 3, where we apply the pulse that the RL-agent found for the qubit frequencies marked by black vertical lines to qubit frequencies in their vicinity. The plots show that the fidelity is maintained up to frequency variations of (5 – 10)%.

Yet, one of the main strengths of the proposed method is that the RL agent can be trained with real experimental data. Crucially this enables training the agent without knowledge of a precise model for the qubits and coupler, and can thus cope with unavoidable imperfections in the characterization of the device. Moreover, this approach can take advantage of the dynamic nature of the experimental data and enables the RL agent to learn and adapt in real-time to the nuanced variations in the experimental setups, e.g. parameter drift.

Another promising avenue is also to use the pulse obtained from RL on a model as an initial guess, which through the rigorous training employed in this study, serves as a well-informed starting point encapsulating valuable insights into the system dynamics and response characteristics. On the basis of this ansatz pulse, further optimization can be applied to minimize any potential model bias due to parameter variation in experimental device. While benefitting from the robustness shown in Fig. 3, this iterative approach fine-tunes the pulse based on empirical feedback from the experiment itself, and hence experimental precision can be greatly enhanced, ultimately leading to more accurate results.

In summary, we illustrate a reinforcement learning (RL)-driven methodology for the design of rapid and non-intuitive pulse sequences to execute a two-qubit CZ-gate within a tunable coupler architecture. The necessity to avoid leakage into non-computational states in quantum gates has so far been understood as a requirement to employ lower pulse amplitudes leading to slower gates. Our investigation breaks this conclusion via a pulse sequence proposed by an artificial agent. It demonstrates that, grounded solely on penalty or reward considerations, the artificial agent can assimilate effective strategies and unveil realistic parameter configurations for the modulation of coupler piecewise constant flux pulses. These machine-discovered pulses strategically leverage leakage to noncomputational basis states, thereby optimizing time protocols and culminating in an ultrafast CZ-gate with an impressively low duration of 11 ns with error rate  $\sim 4 \times 10^{-3}$ . This is an improvement in gate duration of  $\sim 5.5$  and 3 times respectively, compared to the CZ gate implementations with tunable coupler in [36] with a 60 ns long CZ gate and 34 ns in the surface code implementation with Google’s Sycamore processor [13]. The ability to significantly reduce gate time while maintaining a low error rate represents a pivotal step towards the practical implementation of quantum computation protocols, underscoring the high impact and relevance of our proposed RL-driven design approach.

## ACKNOWLEDGEMENTS

This work received support from the German Federal Ministry of Education and Research via the funding program Quantum Technologies—from basic research to the market under Contract No. 13N16182 MUNIQ-SC. It is also part of the Munich Quantum Valley, which is supported by the Bavarian state government, with funds from the Hightech Agenda

Bayern Plus. BS thanks Lukas Heunisch for useful discussions.

---

\* [bjjita.sarma@fau.de](mailto:bjjita.sarma@fau.de)

- [1] M. A. Nielsen and I. L. Chuang, *Quantum Computation and Quantum Information: 10th Anniversary Edition* (Cambridge University Press, Cambridge, England, UK, 2010).
- [2] M. Cerezo, A. Arrasmith, R. Babbush, S. C. Benjamin, S. Endo, K. Fujii, J. R. McClean, K. Mitarai, X. Yuan, L. Cincio, and P. J. Coles, *Nat. Rev. Phys.* **3**, 625 (2021).
- [3] J. Preskill, *Quantum* **2**, 79 (2018), 1801.00862v3.
- [4] F. Arute *et al.*, *Nature* **574**, 505 (2019).
- [5] M. Kjaergaard, M. E. Schwartz, J. Braumüller, P. Krantz, J. I.-J. Wang, S. Gustavsson, and W. D. Oliver, *Annu. Rev. Condens. Matter Phys.* **11**, 369 (2020).
- [6] S. Rosenblum, P. Reinhold, M. Mirrahimi, L. Jiang, L. Frunzio, and R. J. Schoelkopf, *Science* **361**, 266 (2018).
- [7] L. DiCarlo, J. M. Chow, J. M. Gambetta, L. S. Bishop, B. R. Johnson, D. I. Schuster, J. Majer, A. Blais, L. Frunzio, S. M. Girvin, and R. J. Schoelkopf, *Nature* **460**, 240 (2009).
- [8] C. K. Andersen, A. Remm, S. Lazar, S. Krinner, N. Lacroix, G. J. Norris, M. Gabureac, C. Eichler, and A. Wallraff, *Nat. Phys.* **16**, 875 (2020).
- [9] Y. Ma, Y. Xu, X. Mu, W. Cai, L. Hu, W. Wang, X. Pan, H. Wang, Y. P. Song, C.-L. Zou, and L. Sun, *Nat. Phys.* **16**, 827 (2020).
- [10] S. Krinner, N. Lacroix, A. Remm, A. Di Paolo, E. Genois, C. Leroux, C. Hellings, S. Lazar, F. Swiadek, J. Herrmann, G. J. Norris, C. K. Andersen, M. Müller, A. Blais, C. Eichler, and A. Wallraff, *Nature* **605**, 669 (2022).
- [11] E. Knill and R. Laflamme, *Phys. Rev. A* **55**, 900 (1997).
- [12] A. L. Grimsmo and S. Puri, *PRX Quantum* **2**, 020101 (2021).
- [13] R. Acharya *et al.*, *Nature* **614**, 676 (2023).
- [14] Z. Chen, J. Kelly, C. Quintana, R. Barends, B. Campbell, Y. Chen, B. Chiaro, A. Dunsworth, A. G. Fowler, E. Lucero, E. Jeffrey, A. Megrant, J. Mutus, M. Neeley, C. Neill, P. J. J. O'Malley, P. Roushan, D. Sank, A. Vainsencher, J. Wenner, T. C. White, A. N. Korotkov, and J. M. Martinis, *Phys. Rev. Lett.* **116**, 020501 (2016).
- [15] C. C. Bultink, T. E. O'Brien, R. Vollmer, N. Muthusubramanian, M. W. Beekman, M. A. Rol, X. Fu, B. Tarasinski, V. Ostroukh, B. Varbanov, A. Bruno, and L. DiCarlo, *Sci. Adv.* **6**, 10.1126/sciadv.aay3050 (2020).
- [16] R. Fazio, G. M. Palma, and J. Siewert, *Phys. Rev. Lett.* **83**, 5385 (1999).
- [17] K. S. Chou, T. Shemma, H. McCarrick, T.-C. Chien, J. D. Teoh, P. Winkel, A. Anderson, J. Chen, J. Curtis, S. J. de Graaf, J. W. O. Garmon, B. Gudlewski, W. D. Kalfus, T. Keen, N. Khedkar, C. U. Lei, G. Liu, P. Lu, Y. Lu, A. Maiti, L. Mastalli-Kelly, N. Mehta, S. O. Mundhada, A. Narla, T. Noh, T. Tsunoda, S. H. Xue, J. O. Yuan, L. Frunzio, J. Aumentado, S. Puri, S. M. Girvin, M. S. Harvey, Jr., and R. J. Schoelkopf, *arXiv* [10.48550/arXiv.2307.03169](https://arxiv.org/abs/10.48550/arXiv.2307.03169) (2023), 2307.03169.
- [18] F. Yan, P. Krantz, Y. Sung, M. Kjaergaard, D. L. Campbell, T. P. Orlando, S. Gustavsson, and W. D. Oliver, *Phys. Rev. Appl.* **10**, 054062 (2018).
- [19] L. Heunisch, C. Eichler, and M. J. Hartmann, *Phys. Rev. Appl.* **20**, 064037 (2023).
- [20] P. Mundada, G. Zhang, T. Hazard, and A. Houck, *Phys. Rev. Appl.* **12**, 054023 (2019).
- [21] I. Goodfellow, Y. Bengio, and A. Courville, *Deep Learning* (MIT Press, 2016) <http://www.deeplearningbook.org>.
- [22] R. S. Sutton and A. G. Barto, *Reinforcement learning: An introduction* (MIT press, 2018).
- [23] D. Silver, A. Huang, C. J. Maddison, A. Guez, L. Sifre, G. van den Driessche, J. Schrittwieser, I. Antonoglou, V. Panneershelvam, M. Lanctot, S. Dieleman, D. Grewe, J. Nham, N. Kalchbrenner, I. Sutskever, T. Lillicrap, M. Leach, K. Kavukcuoglu, T. Graepel, and D. Hassabis, *Nature* **529**, 10.1038/nature16961 (2016).
- [24] D. Silver, J. Schrittwieser, K. Simonyan, I. Antonoglou, A. Huang, A. Guez, T. Hubert, L. Baker, M. Lai, A. Bolton, Y. Chen, T. Lillicrap, F. Hui, L. Sifre, G. van den Driessche, T. Graepel, and D. Hassabis, *Nature* **550**, 354 (2017).
- [25] M. Krenn, J. Landgraf, T. Foesel, and F. Marquardt, *Phys. Rev. A* **107**, 010101 (2023).
- [26] V. Gebhart, R. Santagati, A. A. Gentile, E. M. Gauger, D. Craig, N. Ares, L. Banchi, F. Marquardt, L. Pezzè, and C. Bonato, *Nat. Rev. Phys.* **5**, 141 (2023).
- [27] M. Bukov, A. G. R. Day, D. Sels, P. Weinberg, A. Polkovnikov, and P. Mehta, *Phys. Rev. X* **8**, 031086 (2018).
- [28] T. Fösel, P. Tighineanu, T. Weiss, and F. Marquardt, *Phys. Rev. X* **8**, 031084 (2018).
- [29] R. Porotti, D. Tamascelli, M. Restelli, and E. Prati, *Commun. Phys.* **2**, 1 (2019).
- [30] B. Sarma, S. Borah, A. Kani, and J. Twamley, *Phys. Rev. Res.* **4**, L042038 (2022).
- [31] S. Borah, B. Sarma, M. Kewming, G. J. Milburn, and J. Twamley, *Phys. Rev. Lett.* **127**, 190403 (2021).
- [32] Z. T. Wang, Y. Ashida, and M. Ueda, *Phys. Rev. Lett.* **125**, 100401 (2020).
- [33] S. Borah and B. Sarma, *Phys. Rev. Lett.* **131**, 210803 (2023).
- [34] V. V. Sivak, A. Eickbusch, B. Royer, S. Singh, I. Tsioutsios, S. Ganjam, A. Miano, B. L. Brock, A. Z. Ding, L. Frunzio, S. M. Girvin, R. J. Schoelkopf, and M. H. Devoret, *Nature* **616**, 50 (2023).
- [35] K. Reuer, J. Landgraf, T. Fösel, J. O'Sullivan, L. Beltrán, A. Akin, G. J. Norris, A. Remm, M. Kerschbaum, J.-C. Besse, F. Marquardt, A. Wallraff, and C. Eichler, *Nat. Commun.* **14**, 1 (2023).
- [36] Y. Sung, L. Ding, J. Braumüller, A. Vepsäläinen, B. Kannan, M. Kjaergaard, A. Greene, G. O. Samach, C. McNally, D. Kim, A. Melville, B. M. Niedzielski, M. E. Schwartz, J. L. Yoder, T. P. Orlando, S. Gustavsson, and W. D. Oliver, *Phys. Rev. X* **11**, 021058 (2021).
- [37] J. Stehlik, D. M. Zajac, D. L. Underwood, T. Phung, J. Blair, S. Carnevale, D. Klaus, G. A. Keefe, A. Carniol, M. Kumph, M. Steffen, and O. E. Dial, *Phys. Rev. Lett.* **127**, 080505 (2021).
- [38] T. Haarnoja, A. Zhou, P. Abbeel, and S. Levine, *arXiv* [10.48550/arXiv.1801.01290](https://arxiv.org/abs/10.48550/arXiv.1801.01290) (2018), 1801.01290.

## Supplemental Material

### TRANSVERSE AND LONGITUDINAL COUPLINGS BETWEEN THE QUBITS

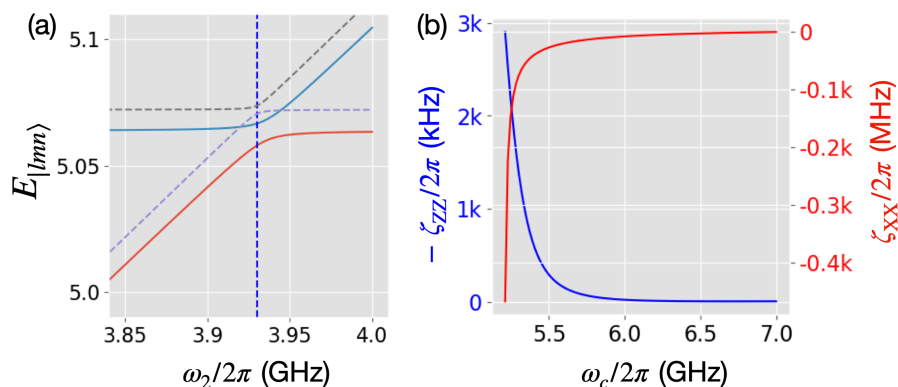


FIG. S1. (a) Avoided level crossing corresponding to the energy splitting given by  $2\zeta_{XX}$  when the effective coupling between the qubits is switched on by varying  $\omega_c$  (solid lines), vs the level crossing at the idle point (dashed lines). (b) The effective static transverse ( $\zeta_{XX}$ ) and longitudinal ( $\zeta_{ZZ}$ ) couplings. The idle point is chosen where both are negligible.

We aim to design the controlled-Z (CZ) gate utilizing the transverse qubit-qubit coupling to induce a phase of  $e^{i\pi}$  in the computational state  $|101\rangle$  by using nonadiabatic transitions to the non-computational eigenstate  $|002\rangle$  and back. As shown in Fig. S1(a), at the idle point, in the dispersive regime where the detuning between the coupler and the qubits is large compared to the couplings, there is level crossing between these two eigenstates. However as the coupler frequency is brought near to that of the two qubits there is avoided crossing as shown in the figure with a gap of  $2\zeta_{XX}$ . Applying a Schrieffer-Wolff transformation, the effective coupler-induced transverse interaction between the data qubits is found as,  $\zeta_{XX} = g_{12} + g_{1c}g_{2c}(\Delta_{1c}^{-1} + \Delta_{2c}^{-1})/2$ , where  $\Delta_{ij} := \omega_i - \omega_j$  denotes the qubit detunings. One can see that, with proper choice of circuit parameters, the effective two-qubit transverse coupling can be tuned and even can be completely switched off, which is the main advantage of such a tunable coupler circuit. We bias our two-qubit gate circuit in a parameter regime where this effective coupling is negligibly small, which is essential for efficient parking of the data qubits. There is also a residual longitudinal (ZZ) interaction because of dispersive shifts in qubit energies caused by the hybridization of qubit wave functions, given by  $\zeta = E_{101} - E_{100} - E_{001} + E_{000}$ , where  $E_{jkl}$  is the energy eigenvalue of the state  $|jkl\rangle$ . Such residual coupling works as crosstalk in the proper implementation of the gate and should be negligible at the parking point of the circuit. We bias the qubits at the frequencies of  $\omega_1/2\pi = 4.2$  GHz,  $\omega_2/2\pi = 5.2$  GHz and  $\omega_c/2\pi = 6.32$  GHz. This results in an almost zero transverse coupling and a negligible zz-crosstalk ( $-8.37$  kHz) (as shown in Fig. S1(b)).

### REINFORCEMENT LEARNING ALGORITHM

Reinforcement Learning (RL) has emerged as a particularly dynamic and important domain within the field of Machine Learning, gaining substantial attention between 2013 and 2016, notably marked by groundbreaking advancements from DeepMind and Google [1, 2]. Although its initial acclaim was in the realm of board games, contemporary research endeavors have broadened its application across diverse technological domains. In the framework of RL, a software agent, denoted as the RL-agent, engages with an environment (referred to as the RL-environment) by systematically observing and executing actions. These actions induce changes in the dynamics of the environment, and reciprocally, the RL-agent receives scalar values in the form of rewards. The overarching objective of the RL-agent is to strategically maneuver within the environment to maximize the cumulative rewards accrued over a specified duration, typically defined as an episode. This approach starkly contrasts with conventional training methods, where machine learning models are trained using pre-existing datasets, either labeled (supervised learning) or unlabeled (unsupervised learning). The unique feature of RL lies in its adaptive and iterative learning process, wherein the RL-agent adjusts its strategy based on real-time consequences within the dynamic environment. This distinctive paradigm shift underscores the evolving nature of RL within the broader spectrum of machine learning methodologies.

The policy of the RL-agent serves as the guiding algorithm for decision-making, and in the domain of deep RL (DRL), it is commonly instantiated through a neural network. This neural network takes observational inputs and produces corresponding action outputs, encapsulating the essence of the RL-agent’s decision strategy. The policy can be classified into two forms: deterministic or stochastic. In the deterministic approach, the action of the RL-agent is precisely determined by the policy parameters, denoted as  $\theta$ , given the state  $s_t$  at time  $t$ . This deterministic relationship is expressed as  $a_t = \mu_\theta(s_t)$ . The RL-agent’s objective is to iteratively refine and optimize these policy parameters ( $\theta$ ) to maximize the cumulative discounted rewards along a trajectory  $\tau = (s_0, a_0, s_1, a_2, \dots)$ , where the discount factor  $\gamma \in (0, 1)$  modulates the significance of future rewards. The optimization process entails maximizing the expected return over discounted rewards, symbolized as  $J(\pi) = \mathbb{E}[R(\tau)]$ , with the ultimate goal of attaining the optimal policy  $\pi^* = \operatorname{argmax}_\pi J(\pi)$ . The RL-agent’s actions are drawn from a probability distribution conditioned on the state  $s_t$ , denoted as  $a_t \sim \pi_\theta(\cdot|s_t)$ .

The concept of the value function in RL revolves around predicting the expected cumulative discounted future reward and assessing the effectiveness of a given state  $s$  or state-action pair  $(s, a)$  in generating a higher net return. The state value  $V_\pi(s) = \mathbb{E}[R_t|s_t = s]$  represents the anticipated return when adhering to policy  $\pi$  from state  $s$ . Conversely, the action value  $Q_\pi(s, a) = \mathbb{E}[R_t|s_t = s, a_t = a]$  signifies the expected return when action  $a$  is executed in state  $s$  followed by policy  $\pi$ . The Bellman equations [3] govern the value functions, which can be self-consistently solved. For instance, the action-value function is expressed as:

$$Q_\pi(s, a) = \mathbb{E} \left[ r(s, a) + \gamma \cdot \max_{a'} Q_\theta(s', a') \right]. \quad (\text{S1})$$

Optimizing the policy encompasses various techniques categorized into three main groups: (a) policy-gradient-based, (b) value-based, and (c) actor-critic-based methods. Value-based approaches, like Q-learning, aim to maximize value functions by solving the Bellman equations. Conversely, policy gradient methods employ gradient descent algorithms to optimize policy parameters, given by:

$$\nabla_\theta J(\pi_\theta) = \mathbb{E} \sum_{t=0}^T \left[ \nabla_\theta \log \pi_\theta(a_t|s_t) \hat{R}_t \right], \quad (\text{S2})$$

where  $\mathbb{E}$  represents the expectation value over the trajectory  $\tau$ . This basic approach can be enhanced by introducing a baseline function,  $b(s_t)$ , to reduce gradient estimation variance, forming the basis of advanced DRL actor-critic algorithms. The objective (loss) function for policy gradient methods to optimize is given by:

$$L^{\text{PG}}(\theta) = \hat{\mathbb{E}}_t \left[ \log \pi_\theta(a_t|s_t) \hat{A}_t \right], \quad (\text{S3})$$

where  $\pi_\theta$  is a stochastic policy, and  $\hat{A}_t = Q(s_t, a_t) - V(s_t)$  is an estimator of the advantage function at timestep  $t$ , considering  $R_t$  as an estimate of  $Q(a_t, s_t)$ . The introduction of the baseline function  $b(s_t)$  aids in reducing gradient estimation variance, forming the foundation of advanced DRL actor-critic algorithms. The objective (loss) function for optimization is:

$$L^{\text{PG}}(\theta) = \hat{\mathbb{E}}_t \left[ \log \pi_\theta(a_t|s_t) \hat{A}_t \right], \quad (\text{S4})$$

where  $\pi_\theta$  is a stochastic policy, and  $\hat{A}_t = Q(s_t, a_t) - V(s_t)$  is an estimator of the advantage function at timestep  $t$ , acknowledging  $R_t$  as an estimate of  $Q(a_t, s_t)$ . An actor-critic algorithm simultaneously learns a policy and a state-value function, utilizing the value function for bootstrapping to reduce variance and expedite learning [3]. The critic updates action-value function parameters, and the actor adjusts policy parameters following the critic’s guidance.

The Soft Actor-Critic (SAC) algorithm is a recently developed actor-critic approach in the realm of RL. What sets SAC apart from other actor-critic methods is its distinctive feature of optimizing the policy in an entropy-regularized manner, rendering it inherently stochastic. In SAC, the policy undergoes training to strike a balance between expected return and entropy. The intentional introduction of entropy serves the purpose of promoting increased exploration and preventing premature convergence of the policy.

At each time step in entropy-regularized RL, the agent is rewarded based on the entropy of the policy distribution,  $\pi^* = \operatorname{argmax}_\pi \mathbb{E}_{\tau \sim \pi} \left[ \sum_{t=0}^{\infty} \gamma^t \left( R(s_t, a_t, s_{t+1}) + \alpha H(\pi(\cdot|s_t)) \right) \right]$ , where  $H(P) = \mathbb{E}_{x \sim P}[-\log P(x)]$  is the entropy of the probability distribution  $P$ , and  $\alpha > 0$  is the trade-off coefficient. The value functions in this setting,  $V^\pi$  and  $Q^\pi$ , are modified accordingly.

$$V^\pi(s) = \mathbb{E}_{\tau \sim \pi} \left[ \sum_{t=0}^{\infty} \gamma^t \left( R(s_t, a_t, s_{t+1}) + \alpha H(\pi(\cdot|s_t)) \right) \middle| s_0 = s \right], \quad (\text{S5})$$

$$Q^\pi(s, a) = \mathbb{E}_{\tau \sim \pi} \left[ \sum_{t=0}^{\infty} \gamma^t R(s_t, a_t, s_{t+1}) + \alpha \sum_{t=1}^{\infty} \gamma^t H(\pi(\cdot|s_t)) \middle| s_0 = s, a_0 = a \right]. \quad (\text{S6})$$

The connection between  $V^\pi$  and  $Q^\pi$  is shown by the equation:

$$V^\pi(s) = \mathbb{E}_{a \sim \pi} [Q^\pi(s, a) + \alpha H(\pi(\cdot|s))]. \quad (\text{S7})$$

The Bellman equation for  $Q^\pi$  is estimated by:

$$Q^\pi(s, a) \approx r + \gamma (Q^\pi(s', \tilde{a}') - \alpha \log \pi(\tilde{a}'|s')), \quad (\text{S8})$$

The approximation of the Bellman equation for  $Q^\pi$  is expressed as:

$$Q^\pi(s, a) \approx r + \gamma (Q^\pi(s', \tilde{a}') - \alpha \log \pi(\tilde{a}'|s')), \quad (\text{S9})$$

In this formulation, the expected values over the next states  $r$  and the states,  $s'$  are taken from the replay buffer, while the subsequent actions  $\tilde{a}'$  are sampled from the policy. Simultaneously, SAC algorithm undergoes the concurrent learning of a policy  $\pi_\theta$  and two Q-functions  $Q_{\phi_1}$  and  $Q_{\phi_2}$ . The loss functions for each Q-function, enforcing the minimum Q-value between the two Q approximators, are articulated as:

$$L(\phi_i, \mathcal{D}) = \mathbb{E}_{(s,a,r,s',d) \sim \mathcal{D}} \left[ \left( Q_{\phi_i}(s, a) - y(r, s', d) \right)^2 \right], \quad (\text{S10})$$

$$y(r, s', d) = r + \gamma \left( \min_{j=1,2} Q_{\phi_{\text{tar}},j}(s', \tilde{a}') - \alpha \log \pi_\theta(\tilde{a}'|s') \right), \quad \tilde{a}' \sim \pi_\theta(\cdot|s'). \quad (\text{S11})$$

Concurrently, SAC learns a policy  $\pi_\theta$  and two Q-functions  $Q_{\phi_1}, Q_{\phi_2}$  while establishing loss functions for each Q-function, with a focus on minimizing the Q-value. The loss is expressed as:

$$L(\phi_i, \mathcal{D}) = \mathbb{E}_{(s,a,r,s',d) \sim \mathcal{D}} \left[ \left( Q_{\phi_i}(s, a) - y(r, s', d) \right)^2 \right], \quad (\text{S12})$$

$$y(r, s', d) = r + \gamma \left( \min_{j=1,2} Q_{\phi_{\text{tar}},j}(s', \tilde{a}') - \alpha \log \pi_\theta(\tilde{a}'|s') \right), \quad \tilde{a}' \sim \pi_\theta(\cdot|s'). \quad (\text{S13})$$

- 
- [1] D. Silver, J. Schrittwieser, K. Simonyan, I. Antonoglou, A. Huang, A. Guez, T. Hubert, L. Baker, M. Lai, A. Bolton, Y. Chen, T. Lillicrap, F. Hui, L. Sifre, G. van den Driessche, T. Graepel, and D. Hassabis, Mastering the game of Go without human knowledge, *Nature* **550**, 354 (2017).
- [2] D. Silver, A. Huang, C. J. Maddison, A. Guez, L. Sifre, G. van den Driessche, J. Schrittwieser, I. Antonoglou, V. Panneershelvam, M. Lanctot, S. Dieleman, D. Grewe, J. Nham, N. Kalchbrenner, I. Sutskever, T. Lillicrap, M. Leach, K. Kavukcuoglu, T. Graepel, and D. Hassabis, Mastering the game of Go with deep neural networks and tree search, *Nature* **529**, 10.1038/nature16961 (2016).
- [3] R. S. Sutton and A. G. Barto, *Reinforcement Learning: An Introduction*, 2nd ed. (The MIT Press, 2018).